Thermo-economic optimization and design of the heat exchangers in the feedwater line of the power conversion system coupled to DEMO fusion reactor

M.J. Montes [a],[*] , D. D'Souza [a] , E. Bubelis [b], S. Perez-Martin [b]

[a] E.T.S. Ingenieros Industriales - UNED, C/Juan del Rosal 12, 28040 Madrid, Spain
[b] Institute for Neutron Physics and Reactor Technology. Karlsruhe Institute of Technology, Hermann-von-Helmholtz-Platz 1, Eggenstein-Leopoldshafen 76344, Germany

ABSTRACT

This article presents a methodology for the thermo-economic optimization of shell-and-tube heat exchangers and its direct application to the design of the heat exchangers in the Feedwater Line of DEMO Power Conversion System, for the Helium-Cooled Pebble Bed Balance of Plant concept.

This optimization consists of minimizing the heat exchanger total present cost comprising both the investment cost and the operating cost related to the pumping power to overcome friction losses while ensuring an efficient heat transfer performance. For the calculation of the investment cost, a detailed and particularized method for Shell-and-Tube heat exchangers is proposed, which provides very accurate values as related to the actual cost of these heat exchangers. For the pumping power calculation, both tube-side and shell-side fluids pressure drops are included. This calculation is performed by an iterative process, which results finally in the determination of all the thermal parameters that characterize the heat exchanger. The final selection of the heat exchanger also includes specific constructive and design constraints of these heat exchangers, which will also be described in this work.

1. Introduction

The current context has highlighted the need to achieve a sustainable, secure and competitive energy supply, independent of fossil fuels, and based on several energy sources. Within this energy mix, fusion power plays a relevant role with the development of several significant projects worldwide: ITER, whose main objective is to demonstrate the feasibility of fusion as a large-scale energy source by means of a 500 MW fusion power plant [1]; Spherical Tokamak for Energy Production (STEP), which aims to deliver electricity from fusion utilizing a compact spherical tokamak design to achieve efficient plasma confinement and sustained fusion reactors [2]; Affordable, Robust, Compact (ARC), which is based on the use of high-temperature superconducting magnets to achieve higher magnetic fields, enabling a more compact and efficient tokamak design [3]; finally, the project European DEMOnstration Fusion Power Plant (EU DEMO) is going to succeed ITER in the pathway towards the commercial production of net electricity from fusion power, achieving a long plasma operation time, demonstrating tritium self-sufficiency and producing net electric output on an industrial scale

[4]. For the design of this plant, lessons learned from ITER have been incorporated, so that the plant performs in a feasible and simple way, with acceptable technical availability [5,6].

In this approach, the design of the Balance of Plant (BoP) is a key element, whose safe and reliable operation is of great importance for the success of the project [7]. The BoP includes both the Primary Heat Transfer System (PHTS) dedicated to the extraction of thermal energy and the Power Conversion System (PCS), that converts this energy into electricity [8,9]. The thermal energy is generated by the plasma and deposited in the Breeding Blanket (BB) [10], Divertor (DIV) [11] and Vacuum Vessel (VV) [12].

Currently, there are two potential configurations for the BoP: the Water Cooled Lithium Lead (WCLL) concept and the Helium-Cooled Pebble Bed (HCPB) concept. Within the HCPB concept, there are four variants: three Direct Coupling Designs (DCD) and one Indirect Coupling Design (ICD). The configuration for the analysis presented in this paper is the ICD, selected as the reference HCPB BoP configuration for the Conceptual Design Phase of the current EUROfusion Framework Program [13,14]. This option is based on an Intermediate Heat Transport System (IHTS) provided with an Energy Storage System (ESS) operating

Acronyms

|	
BB	Breeding Blanket
BoP	Balance of Plant
CAS	Cassette
CELF	Constant-Escalation Levelization Factor
CEPCI	Chemical Engineering Plant Cost Index
COND	Condenser
CRF	Capital Recovery Factor
DCD	Direct Coupling Design
DIV	Divertor
EoL	End of Life
EU DEMO	European DEMOnstration Fusion Power Plant
ESS	Energy Storage System
FWH	Feedwater Heater
HCPB	Helium-Cooled Pebble Bed
HP	High Pressure
HX	Heat Exchanger
IB	Inner Blanket
ICD	Indirect Coupling Design
IHTS	Intermediate Heat Transport System
IHX	Intermediate Heat Exchanger
LP	Low Pressure
MSSG	Molten Salt Steam Generator
MSEP	Moisture Separator
OB	Outer Blanket
OTSG	Once Through Steam Generator
PFC	Plasma Facing Components
PHTS	Primary Heat Transfer System
RH	Reheater
STHX	Shell-and-Tube Heat Exchanger
VV	Vacuum Vessel
WCLL	Water Cooled Lithium Lead

Notation

Latin letters

A	Area (m^2)
B	Baffles spacing (m)
C_b	Cost of the base heat exchanger ($€$ m^{-2})
C_E	Electricity cost ($€$ MWh^{-1})
C_I	Investment cost ($€$)
C_i	Correction factors for the cost
C_O	Operation cost ($€$)
C_T	Total cost ($€$)
D	Shell diameter (m)
d	Tube diameter (m)

ΔP	Pressure drop (Pa)
f	Friction factor / cost multiplier in Purohit method
$\dot{G}$	Fluid mass velocity (kg s^{-1} m^{-2})
g	Gravity acceleration (m s^{-2})
h	Convection heat transfer coefficient (W m^{-2} K^{-1})
h_{lv}	Latent heat of vaporization (J kg^{-1})
i_{eff}	Effective discount rate (%)
J	Correction factor
j	Colburn j-factor
k	Thermal conductivity (W m^{-1} K^{-1})
L	Length (m)
$\dot{m}$	Mass flow rate (kg s^{-1})
n	Economic life of the power plant (years)
N	Number of tubes/baffles
Nu	Nusselt number
P	Pressure (Pa)
p	Cost multiplier in Purohit method
Pr	Prandtl number
$\dot{Q}$	Power (W)
r	Cost multiplier in Purohit method
Re	Reynolds number
r_i	Inflation (%)
r_n	Nominal escalation rate (%)
r_r	Real escalation rate (%)
T	Temperature (°C)
u	Velocity (m s^{-1})
Y	Yearly operation time (hours)

Greek Letters

ε	Rugosity (m)
η	Efficiency
Δ	Increment
ρ	Density (kg m^{-3})
μ	Viscosity (Pa s^{-1})

Subscripts

b	Baffles
e	Equivalent
id	Ideal
l	Liquid
s	Shell
i	Inside surface
max	Maximum
o	Outside surface
t	Tube
v	Vapour
w	Wall

with HITEC molten salt between 270 °C and 465 °C [15,16] to decouple the PHTS from the PCS. This configuration is shown in Fig. 1.

The decoupling between the fusion reactor and the power cycle is necessary as DEMO is characterized by pulsed operation, with two main phases, pulse and dwell. During DEMO's 2-hour pulsed operation, the IHTS simultaneously produces steam in the Molten Salt Steam Generator (MSSG) and also stores a part of the thermal energy from the BB PHTS in the HITEC hot tank. This stored energy is released during the 10-minute dwell DEMO operation, thus supporting continuous steady-state operation at 91.3 % of its nominal power [17]. This is the design point for the cycle, as stated in Section 2.

As previously said, there are three DEMO heat sources coupled to the PCS, whose thermal power can vary slightly through its operation. The main heat source is the Breeding Blanket PHTS, which is coupled to the IHTS via the He-Molten Salt Intermediate Heat Exchanger (IHX). The

two secondary heat sources are available from the Divertor and according to their temperature level are coupled to the low-pressure and the high-pressure feedwater line, respectively. The current values are shown in Table 1, according to the '2021 Energy Map' [18].

The Breeding Blanket PHTS consists of 8 combined Inner Blanket (IB) and Outer Blanket (OB) cooling loops operated with Helium between 300 °C and 520 °C, which represent a total thermal power in the range from 1910 to 2117 MW_{th} during pulse operation. The Divertor (DIV) PHTS consists of two cooling systems: one for the Plasma Facing Components (PFC) and the other one for the Cassette (CAS) supporting structure. During pulse operation, the thermal power removed from DIV-PFC ranges from 170 to 251 MW_{th}, with a temperature decrease from 136 °C to 130 °C, whereas the thermal power from DIV-CAS ranges from 181 to 216 MW_{th} with a temperature decrease from 210 °C to 180 °C, thus delivering power to the PCS feedwater line. Finally, the thermal
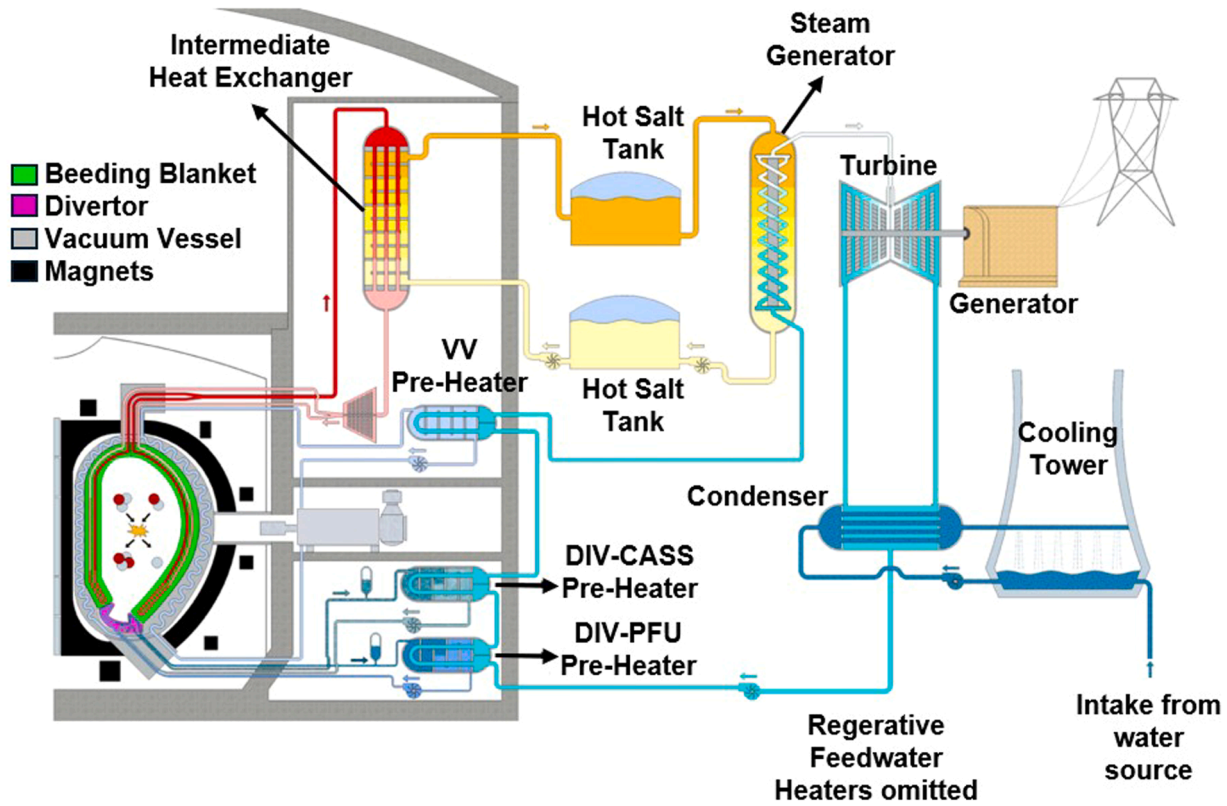
Fig. 1. Simplified scheme of the configuration selected for the Balance of Plant (BoP): Helium-Cooled Pebble Bed (HCPB), Indirect Coupling Design (ICD) (Source: [14]).

Table 1

Characteristics of the heat sources in the EU DEMO PHTS, for the option HCPB BB [17].

Source	BB	DIV-PFC	DIV-CAS	VV
Thermal power range - pulse operation (MW$_{th}$)	1910 - 2117	170 - 251	181 - 216	45 - 48
Inlet temperature (°C)	300	130	180	40
Outlet temperature (°C)	520	136	210	60

Fig. 2. Schematic diagram of a shell-and-tube heat exchanger displaying the fluid-side and the shell-side fluid flow circuits.

power from the Vacuum Vessel (VV) has decreased through the project and the current value ranges from 45 to 48 MW$_{th}$, with an operating temperature decrease from 60 °C to 40 °C. Because of this low-grade operating temperature, it was decided in the new Energy Map [18] to eliminate the integration of VV thermal power into the PCS, thus simplifying the low-pressure feedwater line.

As mentioned in the previous paragraph, the feedwater line of the PCS in the EU DEMO has the peculiarity of not only to perform its original function of preheating the cycle feedwater, but also to incorporate the heat from the secondary sources, DIV-PFC and DIV-CAS, according to the latest configuration. This condition requires careful design of the cycle heat exchangers, which, although they are conventional Shell-and-Tube Heat Exchangers (STHX), must be designed to operate under non-standard conditions.

Shell-and-tube heat exchangers are one of the most common types of heat exchangers used in industrial applications. They consist of a series of tubes embedded in a cylindrical shell. The fluid inside the tubes is referred to as the tube-side fluid, while the fluid through the shell is known as the shell-side fluid. Heat transfer occurs through the tubes wall, from one fluid to the other.

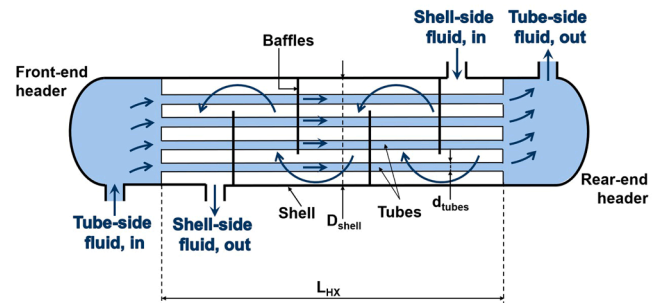Fig. 2 illustrates this type of heat exchanger, as well as its main components.

The aim of this work is to present a methodology to calculate an optimized design of the STHXs of DEMO PCS feedwater line, including the heat exchangers that transfer the heat from the Divertor. To this end, this study has been conducted as follows: firstly, the power cycle used in the HCPB option is presented schematically, with a more detailed description of the STHX included in the feedwater train. Then, a thermo-economic optimization is conducted, balancing the investment cost and the pumping power cost. For that, the thermo-fluid design of each heat exchanger, also accounting for the conventional standards, is performed. The up-to-date investment cost is calculated using a very detailed method that considers both materials and design parameters of STHXs. As will be shown in the results (Section 3), the investment cost estimated by this method is very close to the actual investment cost, compared to other methods based exclusively on the heat exchange area, which underestimate the cost.

2. Methodology

The HX optimization method explained in this Section is general in scope and could be applied to any STHX. However, this optimization has been developed within the framework of the EUROfusion Project, taking as reference a specific PCS configuration described in Section 2.1. This Section also includes a description of the STHXs to be optimized, along with their thermal and constructive constraints. Next, Section 2.2 contains a description of the optimization algorithm used for the design, as well as the objective function to be minimized. Section 2.3 is devoted to the correlations used for the thermal fluid-dynamic design of the heat exchangers. Finally, Section 2.4 presents the Purohit method [19], which is used to estimate the investment cost of these heat exchangers. This method is characterized by being very thorough and providing a cost value very close to the current cost for this type of heat exchanger.

2.1. General configuration of DEMO power conversion system, assuming Helium as primary coolant for blanket cooling

For the DEMO HCPB variant, the Balance of Plant is composed of the IHTS and the PCS. The PCS configuration, on which the heat exchanger sizing calculation is based, is presented in Fig. 3 for the design point conditions [17]. For these conditions, all heat sources coupled to the PCS have been considered to operate at their maximum powers according to Table 1: 2117 MW$_{th}$ for BB, 251 MW$_{th}$ for DIV-PFC and 216 MW$_{th}$ for DIV-CAS.

As shown in Fig. 3, thermal energy recovered from BB-PHTS is the main heat source for the IHTS and then for the PCS, which are coupled though a two-stage MS steam generator. The heat from DIV-PFC is coupled to the Low-Pressure (LP) feedwater line, whereas the heat from DIV-CAS is coupled to the High-Pressure (HP) feedwater line. The steam turbine is constituted by a double-flow HP section and a double-flow LP section. There is one steam extraction from the HP section to feed a Feedwater Heater (FWH). The steam exiting the HP section is directed to the moisture separator (MSEP) and then superheated in the reheater (RH) before entering the LP section. There are two steam extractions from the LP section to feed the deaerator and one FWH, respectively. The feedwater line of the cycle consists of a LP zone and a HP zone, both separated by the deaerator. The condensate pump increases the water pressure to overcome the pressure drop in two HXs in the LP zone: one FWH (FWH$_1$) and one HX transferring the heat from the Divertor (DIV-PFC HX). Thermal power of FWH$_1$ is equal to 40.71 MW$_{th}$, with feedwater temperature increase of ~13 °C. DIV-PFC HX has the peculiarity that the feedwater circulates through the shell, whereas the divertor water circulates through the tubes. The reason for this circulation mode is to provide an additional barrier to avoid any potential contamination of the cycle feedwater, which is rather unlikely due to the existence of an intermediate heat transport system. The thermal power of this heat exchanger is 251 MW$_{th}$ (there are four units in parallel), and the feedwater temperature increment is ~85 °C. Next, the water is introduced into the deaerator, which incorporates a turbine steam extraction from the LP section. At the outlet of the deaerator, the feed pump increases the water pressure so that it reaches the turbine inlet at the required pressure, countering the pressure losses in the other HXs and in the MS steam generator. The first HX after the deaerator is the DIV-CAS HX with a power of 216 MW$_{th}$ (there are 4 units in parallel) and a feedwater increase of ~54 °C. As in the previous secondary-source HX, the water from the divertor circulates inside the tubes, while the feedwater circulates through the shell. Following this HX, there is one feedwater heater (FWH$_2$), with a thermal power of 49.5 MW$_{th}$, and an increase of ~12 °C in the feedwater temperature, so that the water temperature at the inlet of the steam generator is ~211 °C.

In order to design the STHXs presented in the feedwater line, these HXs have been classified into two types:

- Condenser and conventional feedwater heat exchangers (COND, FWH$_1$, and FWH$_2$). These heat exchangers are conventional STHXs in the feedwater line of a PCS, that is, the primary fluid through the tubes is liquid water, whereas the secondary fluid is steam that condenses in the shell.
- Heat exchangers to transfer heat from the secondary sources (DIV-PFC HX and DIV-CAS HX). These heat exchangers are also conventional STHXs, but both the primary and secondary sides contain single-phase fluid.

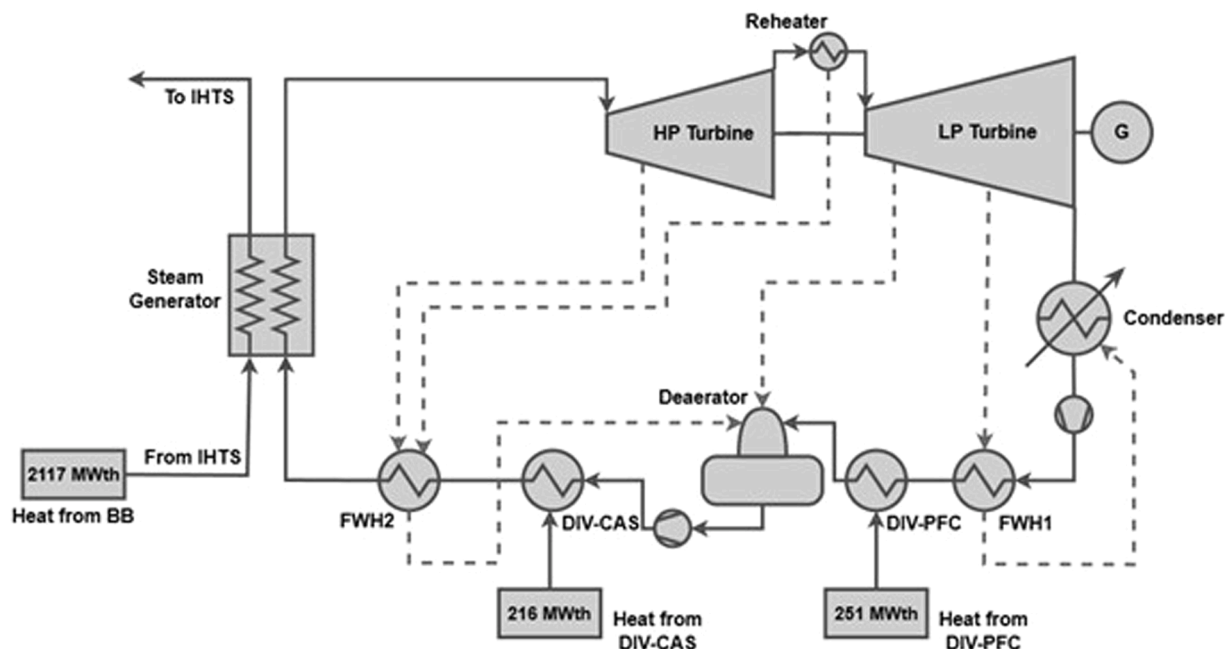Following the project guidelines regarding the systems design [7],

Fig. 3. Simplified scheme of the power conversion system (PCS) for the Helium-cooled pebble bed (HCPB), Indirect coupling design (ICD) configuration (Adapted from: [17]).

the heat exchangers have been designed considering the End of Life (EoL) conditions, in which some of the tubes are plugged (5 % of total tubes for condensers and feedwater heaters; and 10 % of total tubes for DIV-PFC HX and DIV-CAS HX). The equipment fouling factors have been taken from technical references [20,21], and they are summarized in Table 2.

2.1.1. Design of condenser and conventional feedwater heat exchangers: COND, FWH₁ and FWH₂

From the point of view of heat transfer, all these HXs are designed in the same way: the primary fluid going through the tubes is liquid water (from the cold sink in the condenser; pressurized feedwater of the cycle for FWH₁ and FWH₂); the secondary fluid entering the shell is saturated steam, that condenses as it flows through the shell in the case of the condenser, the low-pressure feedwater (FWH₁) and the high-pressure feedwater FWH₂; there is no desuperheating section in any of the feedwater heaters, not even in the HP line, as the steam entering the shell is saturated steam. The correlations used for the thermal fluid-dynamic characterization of the HXs are explained in Section 2.3.

All these HXs have been designed for DEMO pulse operating conditions. Two condenser units have been designed to be located downstream of each of the two double-flow low-pressure turbine cylinders. The condenser has been modelled as one shell pass and two tube passes (1–2) HX. Other possibilities are also valid, but this is the most common. It is advisable to use this design when it is necessary to minimize pressure drop; in this case, due to the large steam mass flow from the turbine, as well as its low pressure, this option seems adequate. The number of baffles in this case is not a crucial issue, as the fluid velocity in the shell is very low, with the objective the pressure drop, so this number is minimized. The tube material (Admiralty metal, ASME: SB 111, SB 395), as well as the normalized diameters have been selected according to bibliographic references [20,21].

The general requirements for the feedwater heaters are taken from technical literature [20–22]:

- Tube material: austenitic steel SA 688 TP304 for welded tubes (low-pressure feedwater heaters); austenitic steel SA 213 TP 304 for seamless tubes (high-pressure feedwater heaters).
- Tube thickness: according to ASME Boiler and Pressure Vessel Code and no <1.2 mm (low-pressure feedwater heaters).
- Water velocity in the tubes: lower than 1.8 m s⁻¹ (low-pressure feedwater heaters); lower than 2.4 m·s⁻¹ (high-pressure feedwater heaters).
- Tube length: lower than 30 m
- The shell-diameter-to-tube-length ratio ranges from 1/15 to 1/5:

$$1/15 < D_s/L_t < 1/5$$

- The baffles spacing ranges from 40 % to 60 % of the shell diameter:

$$0.4 \, D_s < B_{baffles} < 0.6 \, D_s$$

Table 2
Fouling resistances of the shell-and-tube heat exchangers in the feedwater line of the power cycle.

	Fouling resistance ($^\circ$C m² W⁻¹)	
	Tube-side	Shell-side
COND	$1.8 \cdot 10^{-4}$	$0.9 \cdot 10^{-4}$
FWH₁	$1.76 \cdot 10^{-4}$	$0.88 \cdot 10^{-4}$
FWH₂	$1.76 \cdot 10^{-4}$	$0.88 \cdot 10^{-4}$
DIV-PFC	0	$1.76 \cdot 10^{-4}$
DIV-CAS	0	$1.76 \cdot 10^{-4}$

Tube length affects the cost and operation of heat exchangers. Basically, the longer the tube (for any given total surface), the fewer tubes are needed, and the shell diameter decreases as well, resulting in lower cost. There are, of course, several limits to this general rule, best expressed by the shell-diameter-to-tube-length ratio, which should be within limits of about 1/5 to 1/15. Maximum tube length is sometimes dictated by architectural layouts and, ultimately, by transportation to about 30 m. All the feedwater heaters have been modelled as one shell pass and two tube passes (1–2), being the shell of E-type [22]. The thermal and geometrical parameters of these HX are shown in the results (Section 3).

2.1.2. Design of the heat exchangers to transfer heat from the secondary sources: DIV-PFC HX and DIV-CAS HX

The two HXs for the secondary sources operate under highly variable conditions: thermal power during the pulse is very high, whereas it is practically null during the dwell. The HXs are designed for pulse conditions, considering a very high mass flow. These HXs are divided into four units. DIV-PFC HX is modelled as one shell pass and one tube pass (1–1), being the shell of E-type, while DIV-CAS HX is 2–2 and an F-type shell is adopted, in a "U" configuration [22].

As in the previous Section, the other design conditions for these heat exchangers are as follows:

- Tube material: Inconel 690 (seamless) for both HXs.
- Maximum water velocity in the tubes has been set to 3 m·s⁻¹.
- Tube length: lower than 30 m.
- The ratio shell diameter to tube length ranges from 1/15 to 1/5:

$$1/15 < D_s/L_t < 1/5$$

- The baffle spacing ranges from 40 % to 60 % of the shell diameter:

$$0.4 \, D_s < B_{baffles} < 0.6 \, D_s$$

2.2. Methodology for the thermo-economic optimization of the heat exchangers

The optimization process is similar to that described in other works [23,24], in which the objective function to be minimized is the HX cost, including both the investment cost and the operating cost, i.e., the pumping power cost. However, there are important differences in the calculation, as detailed below.

The objective function to be minimized is the annualized total HX cost, according to Eq. (1):

$$C_{T, \, annual} = CRF \cdot C_I + C_{O,annual} = CRF \cdot C_I + CELF \cdot C_E \cdot Y \cdot \dot{Q}_{pumping} \qquad (1)$$

In the above equation, C_I is the total f.o.b (free-on-board) investment cost of the STHX, calculated by means of the Purohit method, explained in Section 2.4; $C_{O, \, annual}$ is the annual operation cost; CRF is the capital-recovery factor and CELF is the constant-escalation levelization factor, both defined below; C_E is the electricity cost, 80.4 $ MWh⁻¹, which is based on the average market price in the USA [25]; Y is the yearly operation time, assuming continuous operation and a capacity factor of 90 % [26]; $\dot{Q}_{pumping}$ is the pumping power to overcome both fluids' pressure drops (through the tubes and the shell), according to Eq. (2).

$$\dot{Q}_{pumping} = \frac{1}{\eta_{pump}} \left(\frac{\dot{m}_t}{\rho_t} \cdot \Delta P_t + \frac{\dot{m}_s}{\rho_s} \cdot \Delta P_s \right) \qquad (2)$$

In Eq. (2), η_{pump} is the pumping power electromechanical efficiency, which typically ranges from 70 % to 90 % in thermal power plants, thus an efficiency of 75 % is considered; $\dot{m}$ is the fluid mass flow through the tubes (t) or the shell (s); ρ is the fluid density and ΔP is the fluid pressure

drop. It is important to note that to calculate both fluids' pressure drops, it is necessary to estimate the thermal performance and size of each heat exchanger, which follows an iterative process explained in Section 2.3.

At this point, it is necessary to highlight a relevant consideration. As in other similar optimization studies, the density considered for Eq. (2) is typically that of the fluid at the STHX inlet conditions. While this assumption holds in most situations, in certain cases it is necessary to account for the entire layout in which the STHX is integrated - namely, the PCS in this case -, where only two pumps are included in the cycle to overcome the pressure drop. Specifically, the pressure drop of the steam exhausted from the turbine and entering the condenser, as well as the HP steam extraction entering FWH$_2$, is compensated by the feed pump, whereas the pressure drop of the LP steam extraction entering FWH$_1$ is overcome by the condensate pump. Correspondingly, the density considered for each STHX is that of the liquid water at the inlet of these pumps, which is considerably higher than that of the steam, thereby resulting in a lower pumping power requirement.

The capital-recovery factor (CRF) and the constant-escalation levelization factor (*CELF*) are calculated by means of Eq. (3) and Eq. (4).

$$CRF = \frac{i_{eff} \cdot (1 + i_{eff})^n}{(1 + i_{eff})^n - 1} \quad (3)$$

$$CELF = CRF \cdot \frac{k \cdot (1 - k^n)}{(1 - k)}, \ k = \frac{1 + r_n}{1 + i_{eff}} \quad (4)$$

In the above equations, i_{eff} (%) is the effective discount rate, and *n* is the economic life of the power plant, that has been set to 30 years; r_n is the nominal escalation rate, which represents the annual change in cost and includes the effects of both the real escalation rate r_r and the inflation rate r_i. The values of the parameters defined above are summarized in Table 3.

Finally, the optimization algorithm is shown in Fig. 4.

As observed in Fig. 4, the optimization process will be as follows:

- The optimization variables, with the values assigned iteratively by the optimization algorithm, are the tube outside diameter d_o, and tube-side maximum velocity, $u_{t,\max}$. As the tube diameter is varied, several parameters will also change depending on this diameter.
- The design parameters required by the PCS are established: required thermal duty; mass flow rate of both fluid streams; tube-side fluid inlet/outlet temperature and inlet pressure; shell-side fluid inlet/outlet temperature and inlet pressure. The tube-side and shell-side fluid outlet pressure depend on the particular STHX configuration, calculated by means of a thermo-fluid design routine.
- There are also several fixed parameters defined within the project [7], whose values have been summarized in Sections 2.1 and 2.2, i.e.: the tube-side and shell-side fouling resistances, the shell type, the number of tube-side passages (1,2, 4…), the tubesheet patterns (triangular or square) and pitch.
- Based on the actual values of both design specifications and fixed parameters, as well as the current values of the optimization variables, the STHX thermo-fluid design routine determines the values of the shell-side and tube-side convection heat transfer coefficients (h_s and h_t, respectively), the overall heat transfer coefficient (*U*), the heat transfer area (*A*), the number of tubes (N_t), the tube length (L_t) and finally, the pressure drops (ΔP_t and ΔP_s, respectively), thus
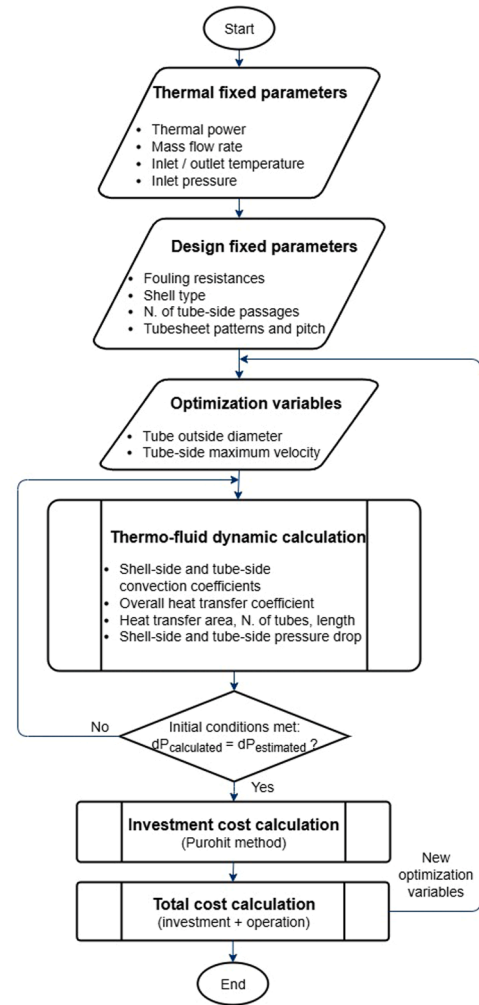

Fig. 4. Proposed algorithm to calculate the optimized design that minimizes the annualized cost of each shell-and-tube heat exchanger in the feedwater line of the power cycle.

defining all constructive details of the HX satisfying the assigned thermal duty specifications. The computed values of fluid pressure losses and the constructive details of the exchanger structure are then used to evaluate the objective function, the annualized total cost of the heat exchanger (Eq. (1)).
- The final design selected will meet the condition of minimal STHX annualized cost, within the constructive constraints in terms of tube length and shell diameter-to-tube length ratio, explained in Section 2.1.

2.3. Thermal fluid-dynamic model of shell-and-tube heat exchangers

For all the STHXs proposed, the fluid in the tubes is always liquid water; the fluid in the shell is water-steam for the condenser, FWH$_1$ and FWH$_2$, whereas it is liquid water in the case of DIV-PFC and DIV-CAS.

The correlations used to calculate the heat transfer, and the pressure drop in the tube-side are the Gnielinski correlation and the Darcy-Weisbach equation [20], respectively. For the heat transfer in the shell-side, the Chen correlation is used when the fluid is water-steam, and condensation occurs on the tube external surface [21]. If the fluid in the shell is liquid water, two equations can be used to calculate the convection heat transfer: Mc Adams correlation and the Bell-Delaware method [20]. These correlations have been implemented and compared, proving that Bell-Delaware method leads to more conservative values of the heat transfer area, so this method has been chosen.

Table 3
Parameters for the thermo-economic optimization of STHXs.

Economic parameters	Value
Effective discount rate i_{eff} (%)	7
Capital recovery factor CRF (year^{-1})	0.0806
Nominal escalation rate (%)	5
k (%)	98.13
Constant-escalation levelization factor (CELF)	1.8287

Finally, pressure drop in the shell-side is calculated by the Bell-Delaware method [20]. Tables 4 and 5 summarize the above equations, which are explained in detail in technical literature [20,21].

In Table 4, Gnielinski correlation employs the following values [20]: Nu_t is the tube-side Nusselt number; f is the friction factor for Gnielinski correlation (smooth tubes); Pr_t is the tube-side fluid Prandtl number; Re_{di} is the tube-side fluid Reynolds number based on the tube inside diameter; ΔP_t is the tube-side fluid pressure drop; f_t is the tube-side fluid friction factor; L_t is the tube length; ρ_t is the tube-side fluid density; u_t is the tube-side fluid velocity; ε is the tube rugosity; and d_i is the tube inside diameter.

In Table 5, Chen correlation employs the following values [21]: Nu_s is the shell-side fluid Nusselt number; h_s is the shell-side fluid heat transfer coefficient; g is the gravity acceleration; ρ_s is the shell-side fluid density; μ_s is the shell-side fluid viscosity; k_s is the shell-side fluid thermal conductivity; h_{lv} is the shell-side fluid modified latent heat; d_o is the tube outside diameter; N_t is the number of tubes; T_{sat} is the saturation temperature; and $T_{s,w}$ is the tube outside wall temperature; finally, subindex s stands for the shell; subindex l stands for liquid, at the film temperature; subindex v stands for vapour, at the saturation temperature. Bell-Delaware method employs the following parameters: $h_{s,id}$ is the ideal shell-side fluid heat transfer coefficient for pure crossflow in an ideal tube bank, modified by the correction factors J_c, J_l, J_b, J_s and J_r, whose calculation is explained in [20]; j_i is the Colburn j-factor for an ideal tube bank; c_{ps} is the shell-side fluid specific heat; $\dot{m}$ is the shell-side fluid mass flow; A_s is the crossflow area at the centreline of the shell for one crossflow between two baffles; $\mu_{s,w}$ is the shell-side fluid viscosity, at the shell inside wall temperature; other symbols appearing in this correlation stands for the same parameters as in the previous Chen correlation. Finally, ΔP_s is the shell-side fluid pressure drop and it is calculated by Bell-Delaware method [20] as the sum of three components: pressure drop in the interior crossflow section, ΔP_c; pressure drop in the window, ΔP_w: and pressure drop in the entrance/exit sections, ΔP_e; N_b is the number of baffles; N_{cw} is the number of tube rows crossed in each baffle window; N_c is the number of tube rows crossed during flow through one crossflow in the HX; ΔP_{bi} is the pressure drop in an equivalent ideal tube bank in one baffle compartment of central baffle spacing; ΔP_{wi} is the pressure drop in an equivalent ideal tube bank in the window section; R_b is the correction factor for bypass flow; R_l is the correction factor for baffle leakage effects; R_s is the correction factor for the entrance and exit section having different baffle spacing than the internal sections; f_i is the shell-side Fanning friction factor; $\dot{G}_s$ is shell-side fluid mass velocity; other symbols appearing in this correlation stands for the same parameters as in the previous correlations.

As already explained, the thermo-fluid HX characterization, for each value of the optimization variables (d_o, and $u_{t,\max}$) results in the necessary parameters for calculating the cost of the heat exchanger: the heat transfer area and other design parameters for estimating the f.o.b investment cost, as well as the tube length to calculate the pumping power.

Table 4
Correlations to calculate heat transfer and pressure drop in the tube-side of the shell-and-tube heat exchangers.

Tube-side convection heat transfer	
Gnielinski correlation [20]	Validity
$Nu_t = \dfrac{(f/8)\,(Re_{di}-1000)\,Pr_t}{1+12.7\left(\sqrt{\frac{f}{8}}\right)\left(Pr_t^{2/3}-1\right)}\left(\dfrac{Pr_t}{Pr_{t,w}}\right)^{0.11}$	$2300 \leq Re_{di} \leq 5\cdot10^6$
$f = \left(1.82\,log_{10}(Re_{di}) - 1.64\right)^{-2}$	
Tube-side pressure drop	
Darcy-Weisbach equation [20]	Validity
$\Delta P_t = \dfrac{1}{2}\,f_t\left(\dfrac{L_t}{d_i}\right)\rho_t\,u_t^2$	$4000 \leq Re_{di} \leq 10^8$ *Rough-pipe regime*
$f_t = \dfrac{0.25}{\left[log_{10}\left(\frac{\varepsilon/d_i}{3.7}+\frac{5.74}{Re_{di}^{0.9}}\right)\right]^2}$	

Table 5
Correlations to calculate heat transfer and pressure drop in the shell-side of the shell-and-tube heat exchangers (*Specific calculation of correction factors J_c, J_b, J_b, J_s and J_r in [20]).

Shell-side convection heat transfer	
Chen correlation for condensation on horizontal tubes [21]	Validity
$Nu_s = \dfrac{h_s\,d_o}{k_{s,l}} = 0.728\cdot\left[\dfrac{g\,\rho_{s,l}\,(\rho_{s,l}-\rho_{s,v})\,h'_{lv}\,d_o^3}{N_t\,\mu_{s,l}\,k_{s,l}\,(T_{sat}-T_{s,w})}\right]^{1/4}$	*Laminar convection* $Ja_s \leq 0.1$ $1 \leq Pr_s \leq 100$
Bell-Delaware method for monophasic fluid [20]	Validity
$h_s = h_{id}\,J_c J_l\,J_b\,J_s\,J_r*$	$Re_{Ds} \leq 10^6$
$h_{id} = j_{id}\,c_{ps}\left(\dfrac{\dot{m}_s}{A_s}\right)\left(\dfrac{k_s}{c_{ps}\,\mu_s}\right)^{2/3}\left(\dfrac{\mu_s}{\mu_{s,w}}\right)^{0.14}$	
Shell-side pressure drop [20]	
Bell-Delaware method	Validity
$\Delta P_s = \Delta P_c + \Delta P_w + \Delta P_e$	$100 \leq Re_{Ds} \leq 10^6$
$\Delta P_s = [(N_b-1)\,\Delta P_{bi}\,R_b + N_b\,\Delta P_{wi}]\,R_l + 2\Delta P_{bi}\left(1+\dfrac{N_{cw}}{N_c}\right)R_b\,R_s$	
$\Delta P_{bi} = 4\,f_i\,\dfrac{\dot{G}_s^2}{2\rho_s}\left(\dfrac{\mu_{s,w}}{\mu_s}\right)^{0.14}$	

The thermal fluid-dynamic characterization is an iterative process, since the pressure drop is unknown, so it is necessary to estimate an initial for the fluid outlet pressure, both for the tube-side and the shell-side, and then compare the calculated pressure drop to the estimated one, reinitiating the process if necessary.

2.4. Method for calculating the cost of shell-and-tube heat exchangers

All the HXs in the feedwater line are conventional shell-and-tube heat exchangers, so the Purohit method has been selected to calculate their cost [19]. This method is very comprehensive as it introduces correction factors that account for the design and materials of the heat exchanger. Although there are other simpler methods that calculate the cost using only the heat transfer area [27], it has been demonstrated that this method produces values comparable to the actual costs of this type of heat exchanger [28]. Purohit method is detailed in the following text.

The STHX cost depends on TEMA type [22], dimensions (shell diameter, tube length and diameter), geometry (gauge, pitch, layout, number of tube passes), construction (welded or seamless), operating conditions (shell-side and tube-side design pressures) and materials. Eq. (5) is used for estimating the cost of the base heat exchanger, C_b ($/m^2$).

$$C_b = \left[\dfrac{6.6}{1 - e^{-\frac{(7-D_s/0.0254)}{27}}}\right]p\cdot f\cdot r \qquad (5)$$

In Eq. (5), D_s is shell diameter, p is a cost multiplier for tube outside diameter, pitch and layout angle, f is a cost multiplier for TEMA-type front head and r is a cost multiplier for TEMA type rear head, whose value is reported in [19]. The base shell-and-tube exchanger is a TEMA E type, welded 14 BWG, average wall, 6.1 m length, 1 tube pass, shell-side and tube-side design pressure $< 1.034\cdot10^6$ Pa, and carbon steel material for every component. Eq. (5) is obtained based on an analysis of the purchase prices of many shell-and-tube exchangers received by means of competitive bids during 1982. This base cost must be corrected considering the correction factors explained in Table 6.

In Table 6, D_s is the shell diameter; L is the tube length; d_o is tube outside diameter; *pitch* is the tube pitch.

Once all the correction factors have been calculated, the f.o.b. (free-on-board) investment cost, C_I, is estimated by Eq. (6).

$$C_I = 10.764\cdot C_b\cdot(1+C_F)\cdot A \qquad (6)$$

In Eq. (6), $C_F = \sum_i C_i$ is the sum of all the cost correction factors previously indicated, A is the heat transfer area. The estimated f.o.b. cost refers to January 1982, the date on which Purohit study was published

Table 6

Correction factors applied to the base shell-and-tube heat exchanger cost, C_b [19].

Correction Factor, C_i	Calculation
C_s: correction factor for shell type. C_s accounts for TEMA shell types different than E-type (base HX)	Values tabulated in a table [19]
C_x: correction factor for expansion joint. C_x accounts for an expansion joint incorporated into the shell of a fixed-tubesheet (base HX)	Values represented in a graph [19]
C_{lt}: correction factor for tube length. C_{lt} accounts for tube length different from 6.1 m (base HX)	$C_{lt} = \left[1 - \dfrac{L}{6.1}\right]\left[1.5 - \dfrac{0.002083 \cdot (D_s/0.0254 - 12)}{1 - (L/6.1)}\right]$ for tube length < 6.1 m $C_{lt} = 0$, for tube length $\geq$ 6.1 m
C_{Ntp}: correction factor for tube passes. C_{Ntp} accounts for tube passes different from 1 (base HX)	$C_{Ntp} = \dfrac{Ntp - 1}{100}$
C_{Ps} / C_{Pt}: correction factors for shell-side / tube-side design pressure C_{Ps} / C_{Pt} accounts for design pressures higher than $1.034 \cdot 10^6$ Pa (base HX)	$C_{Ps} = \left[\dfrac{P_s}{1.034 \cdot 10^6} - 1\right][0.07 + 0.0016\,(D_s/0.0254 - 12)] + X$ $C_{Pt} = \left[\dfrac{P_t}{1.034 \cdot 10^6} - 1\right][0.035 + 0.0056\,(D_s/0.0254 - 12)]$ $X = 0$, for $P_s < 1.38 \cdot 10^7$ Pa X is a graphical function of D_s [18], for $P_s \geq 1.38 \cdot 10^7$ Pa [19]
C_{Mt}: correction factor for tube material C_{Ms}: correction factor for shell material C_{Mch} correction factor for channel material C_{Mtsh}: correction factors for tubesheet material C_{Mt} accounts for tubing cost (welded or seamless) relative to welded carbon steel tubes of the same diameter, wall thickness and cut length (base HX) C_{Ms} accounts for shell cost relative to carbon steel plate of the same dimensions (base HX) C_{Mch} accounts for channel cost relative to carbon steel channel of the same dimensions (base HX) C_{Mts} accounts for tubesheet cost relative to carbon steel tubesheet of the same dimensions (base HX)	$C_{Mt} = y\,(M_1 - 1)$ $C_{Ms} = 0.1\,(M_2 - 1)$ $C_{MCh} = 0.06\,(M_2 - 1)$ $C_{Mtsh} = 0.04\,(M_2 - 1)$ $y = 0.129 + 0.0016\,(D_s/0.0254 - 12)\left[\dfrac{d_o/0.0254}{0.75 \cdot a \cdot pitch^2}\right]$ $a = 1$ for 45° or 90° layouts $a = 0.85$ for 30° or 60° layouts M_1: values tabulated in [19] M_2: values tabulated in [19]
C_G: correction factor for tube gauge C_G accounts for gage metrics different from 14 BWG (base HX)	$C_G = y\,(g - 1)$ y: calculated for C_{Mt} g: cost multiplier for tube gage, values graphically represented in [19]

[19]. All the tables summarizing the main cost parameters for each of the optimized STHX are included in the following Section 3.

The investment cost calculated in Eq. (6) provides a reasonable estimate; however, some discrepancies with actual data were observed when the heat transfer area is large, as in the case of power plant condensers. In such cases, several studies [29,30] have recommended the use of a scaling exponent greater than 0.8 applied to the heat transfer area. A final value of 0.95 has been adopted, based on verification against updated STHX prices reported in [31]. Accordingly, the f.o.b investment cost is modified as shown in Eq. (7).

$$C_{I,modified} = 10.764 \cdot C_b \cdot (1 + C_F) \cdot A^{0.95} \tag{7}$$

Both the STHX investment costs obtained using the original Purohit method and those calculated with the modified Purohit method will be presented in Section 3.

3. Results

The methodology explained in Section 2 has been applied to the optimization of the STHXs in the feedwater line of DEMO HCPB-BoP Power Conversion System. At this point, it should be noted that this calculation methodology is of a general nature, and it can be applied to obtain the optimal design for any type of STHX.

In all cases, the calculation of the minimum STHX total cost leads to an ideal contour map representing the total cost as a function of the tube outside diameter, d_o (y-axis), and the tube-side maximum velocity, $u_{t,max}$ (x-axis). Nevertheless, in this contour map, there are theoretical STHX designs that, while minimizing cost, do not meet certain technical constraints. These constructive and manufacturing constraints have been explained in previous Sections 2.1.1 and 2.1.2. Some of these restrictions refer directly to the tube outside diameter or the tube-side maximum velocity, and they have already been applied when defining the range of these optimization variables for each HX. Specifically, Fig. 5 shows the two most important constraints applied to the condenser: (1) tube length <30 m, resulting in a shaded region of possible designs; (2) shell-diameter-to-tube-length ratio ranging from 1/15 to 1/5, resulting in another shaded region of possible designs. The intersection of both regions yields an overlapping, smaller area of possible designs, on which the cost level lines are plotted. The design corresponding to the lowest cost within this area is selected.

The following figures display the total cost level lines and the region meeting technical constraints for each of the STHE considered: condenser (Fig. 6), feedwater heater FWH$_1$ (Fig. 7), heat exchanger DIV-PFC (Fig. 8), heat exchanger DIV-CAS (Fig. 9) and feedwater heater FWH$_2$ (Fig. 10).

As a result of the previous figures, Table 7 shows the outside tube diameter and tube-side maximum velocity chosen for each of the STHXs studied. Table 8 summarizes all the geometric and thermal parameters for these heat exchangers.

Finally, Table 9 shows the total STHX cost, including the correction factors calculated according to the Purohit method.

As said in Section 2, the estimated f.o.b. cost calculated by Purohit method is referred to 1982 [19]. Nevertheless, the f.o.b. costs showed in Table 9 have been updated to September 2024 using the Chemical Engineering Plant Cost Index (CEPCI) [32], for HXs: $CEPCI_{HX,Sept2024} = 792.5$ and $CEPCI_{HX,1982} = 336.2$. Besides that, the conversion US Dolar (\$) to Euro (€) is also referred to September 2024: $Change\_\$\_to\_€_{Sept2024} = 0.89827$. The last two rows of Table 9 provide the total cost of each STHX, calculated by the original Purohit method summarised in Eq. (6), as well as the modified version with a scaling exponent of 0.95 applied to the heat transfer area, as expressed in Eq. (7). From these values, it can be concluded that the net impact of the scaling exponent increases with the size and cost of the STHX.

4. Discussion

The results presented in Figs. 6–10 provide highly insightful information that can be broadly applied to shell-and-tube heat exchangers. A comprehensive analysis of the graphs reveals two different patterns: for the condenser and feedwater heater FWH$_1$, the contour lines are almost
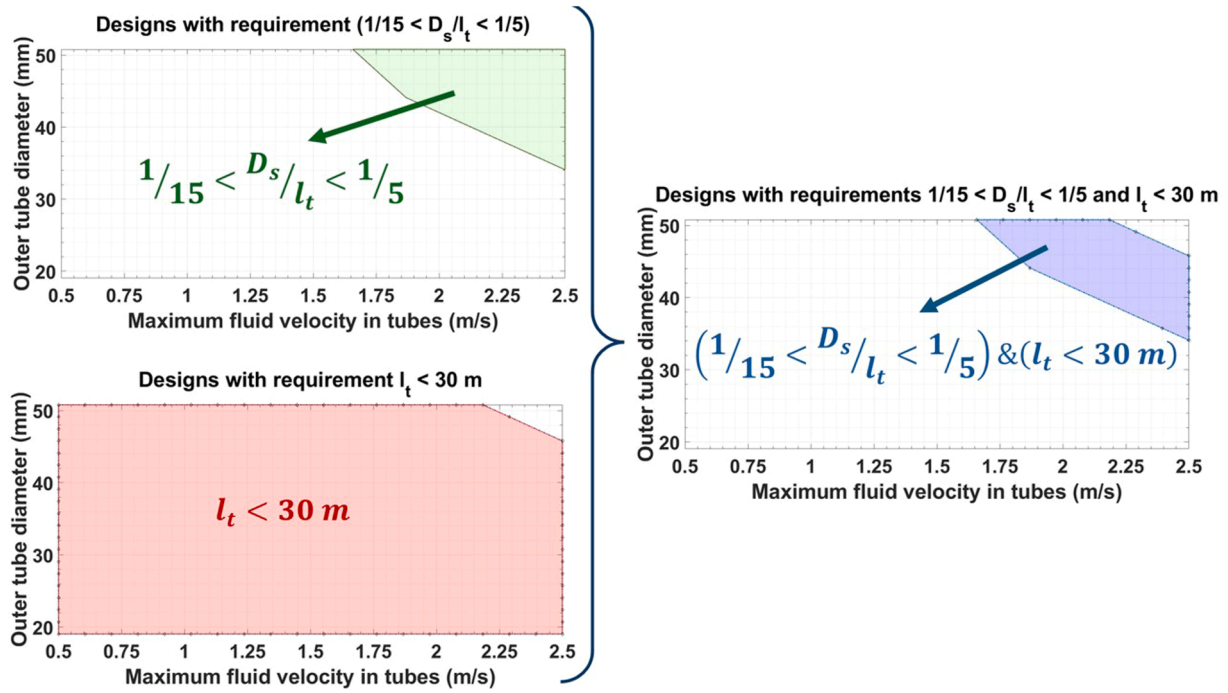
Fig. 5. Shaded areas of possible condenser designs that meet the constructive and manufacturing constraints referring to maximum tube length and ratio shell diameter-to-tube length.
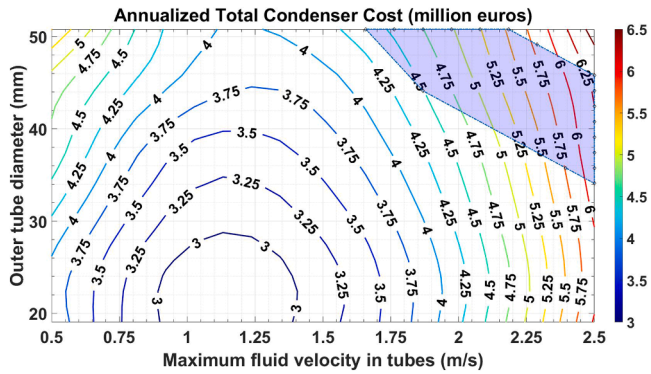

Fig. 6. Annualized total condenser cost, as a function of the outside tube diameter and the tube-side maximum velocity, including constructive and manufacturing constraints (possible designs within the shaded area).

Fig. 8. Annualized total DIV-PFC cost, as a function of the outside tube diameter and the tube-side maximum velocity, including constructive and manufacturing constraints (possible designs within the shaded area).
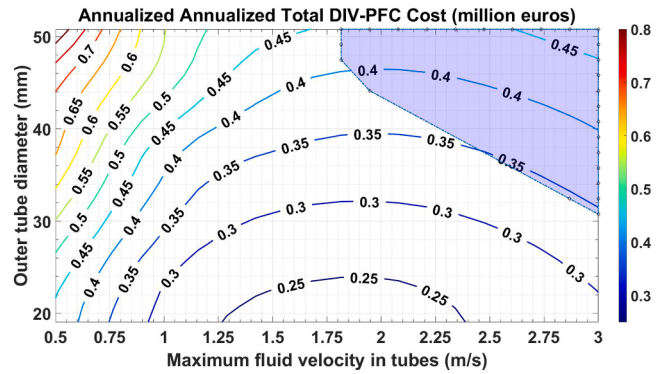

Fig. 7. Annualized total FWH$_1$ cost, as a function of the outside tube diameter and the tube-side maximum velocity, including constructive and manufacturing constraints (possible designs within the shaded area).

Fig. 9. Annualized total DIV-CAS cost, as a function of the outside tube diameter and the tube-side maximum velocity, including constructive and manufacturing constraints (possible designs within the shaded area).
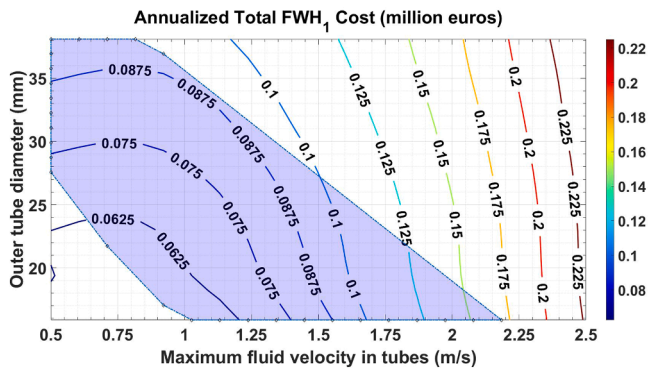
Fig. 10. Annualized total FWH$_2$ cost, as a function of the outside tube diameter and the tube-side maximum velocity, including constructive and manufacturing constraints (possible designs within the shaded area).
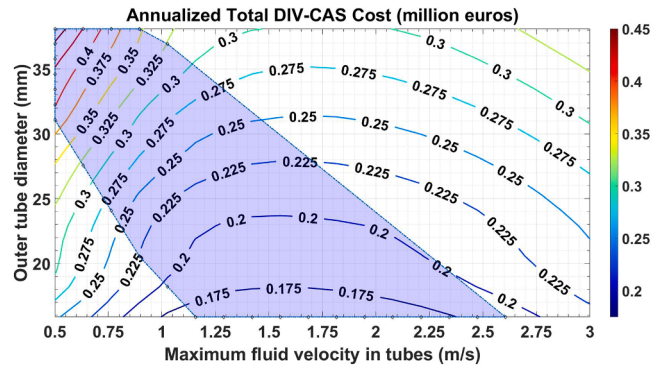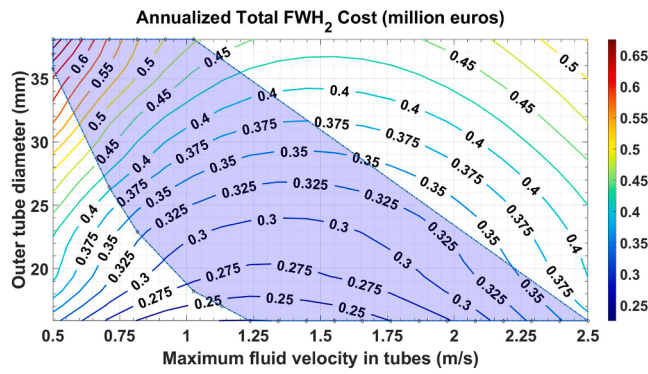
Table 7

Optimum outside tube diameter and tube-side maximum velocity for each shell-and-tube heat exchanger in the feedwater line of the power cycle.

STHX	Outside diameter (mm)	Tube dimensional data (normalized)	Tube-side maximum velocity (m/s)
COND	50.8	2 BWG 18	2
FWH$_1$	15.875	5/8 BWG 18	1
DIV-PFC	31.75	11/4 BWG 18	3
DIV-CAS	15.875	5/8 BWG 18	1.5
FWH$_2$	15.875	5/8 BWG 18	1.5

vertical, indicating lower annualized costs at lower tube-side maximum velocity. In contrast, for the source HXs (DIV-PFC HX and DIV-CAS HX) and the feedwater heater FWH$_2$, these lines tend to be horizontal, suggesting that in these heat exchangers, the dependence on the tube-side maximum velocity is less significant. This is consistent with the velocities reported in the technical literature (Section 2.1.1), which tend to indicate lower velocities for low-pressure STHXs. It should also be noted that, although the DIV-PFC HX is located in the low-pressure region of the feedwater line, it should be considered a high-pressure HX due to its working pressures: the divertor water at 39 bar circulates through the tubes, while the feedwater at 4 bar flows through the shell.

The effect of the two parameters considered for the annualized cost is explained below: the tube-side maximum fluid velocity and the tube diameter. For better understanding, the annualized cost equation, Eq. (8) is recalled here for clarity. It should also be noted that the investment cost mainly depends on the heat transfer area, while the pumping power is primarily influenced by the pressure drop and the density of the fluids circulating through the tubes and the shell.

$$C_{T,\ annual} = CRF \cdot C_I + C_{O,annual} = CRF \cdot C_I + CELF \cdot C_E \cdot Y \cdot \dot{Q}_{pumping} \qquad (8)$$

When the tube-side fluid velocity is increased while keeping the diameter constant, the heat transfer area decreases due to improved heat transfer, and the number of tubes is also reduced. However, the pumping power increases as the pressure drop rises, both on the tube-side and the shell-side. The latter is caused by a reduction in the shell diameter due to the decreased number of tubes.

The effect of the diameter is less significant and practically negligible for low-pressure STHXs. For all STHXs, an increase in diameter at constant velocity leads to an increase in the heat transfer area, as the heat transfer efficiency decreases. This effect is not offset by the reduction in

Table 8

Geometric and thermal characteristics for each shell-and-tube heat exchanger in the feedwater line of the power cycle.

	COND	FWH$_1$	DIV-PFC	DIV-CAS	FWH$_2$
Sizing and geometrical characteristics					
Number of units	2	1	4	4	1
Outer diameter (mm)	50.80	15.875	31.75	15.875	15.875
Thickness (mm)	1.24	1.24	1.24	1.24	1.24
Tube pitch size (mm)	63.50	19.84	39.69	19.84	19.84
Baffle spacing (m)	1.3	1.2	1	0.9	1.2
Pitch-tube layout	Triangular	Triangular	Triangular	Triangular	Triangular
Number of tube passes	2	2	1	2	2
Number of shell passes	1	1	1	2	1
Number of tubes (BoL)	7682	5668	1491	2439	5321
Heat transfer area (m^2)	68.29·10^3	3.38·10^3	1.32·10^3	1.28·10^3	4.16·10^3
Length (m)	27.85	5.97	8.86	5.26	7.84
Shell diameter (m)	8.74	2.35	1.67	1.54	2.27
Thermal characteristics					
Thermal power (MW$_{th}$)	778. 7	40.71	64.65	54.06	49.50
Global Heat Transfer Coefficient (W m^{-2} °C^{-1})	1.48·10^3	1.3·10^3	1.64·10^3	2.13·10^3	1.64·10^3
Primary					
Maximum velocity (m s^{-1})	2	0.5	3	1.5	1.5
Primary inlet temperature (°C)	20	31.79	136	210	199.80
Primary inlet pressure (kPa)	250	421.5	3900	3400	5948.30
Primary mass flow rate (kg s^{-1})	26,682.44	752.23	2528.38	403.62	918.57
Primary outlet temperature (°C)	27.00	44.78	130	180	211.78
Primary outlet pressure (kPa)	188.93	404.57	3862.49	3375.49	5911.63
Primary pressure drop (kPa)	61.07	16.93	37.51	24.51	36.67
Convection heat transfer coefficient (tube-side) (W m^{-2} °C^{-1})	8.19·10^3	6.59·10^3	25.95·10^3	18.44·10^3	19.72·10^3
Fouling Resistance (m^2 °C W^{-1})	1.8·10^{-4}	1.76·10^{-4}	0	0	1.76·10^{-4}
Secondary					
Maximum velocity (m s^{-1})	1.5	1.5	1.5	1.5	1.5
Secondary inlet temperature (°C)	31.78	49.08	44.78	145.85	214.62
Secondary inlet pressure (kPa)	4.7	11.80	404.57	5958	2090.30
Secondary mass flow rate (kg s^{-1})	367.15	17.94	180.43	229.47	122.05
Secondary outlet temperature (°C)	29.89	41.72	129.94	199.87	214.61
Secondary outlet pressure (kPa)	4.27	11.72	402.25	5948.30	2090.16
Secondary pressure drop (kPa)	0.43	0.08	2.32	9.70	0.14
Convection heat transfer coefficient (shell-side) (W m^{-2} °C^{-1})	3.87·10^3	5.8·10^3	3.27·10^3	7.23·10^3	7.43·10^3
Fouling Resistance (m^2 °C W^{-1})	0.9·10^{-4}	0.88·10^{-4}	1.76·10^{-4}	1.76·10^{-4}	0.88·10^{-4}

Table 9

Total cost for each shell-and-tube heat exchanger in the feedwater line of the power cycle.

	COND	FW$_1$	DIV-PFC	DIV-CAS	FW$_2$
Sizing parameters					
Tube material	SB 111	SA 688	Inconel 690	Inconel 690	SA 213
Outer diameter (mm)	50.80	15.875	31.75	15.875	15.875
Tube pitch size (mm)	63.50	19.84	39.69	19.84	19.84
Pitch-tube layout	Triangular	Triangular	Triangular	Triangular	Triangular
Number of tube passes	2	2	1	2	2
Standard TEMA shell type	–	E	E	F	E
Heat transfer area (m^2)	68.89·10^3	3.38·10^3	1.32·10^3	1.28·10^3	4.16·10^3
Length (m)	27.85	5.97	8.86	5.26	7.84
Shell diameter (m)	8.74	2.35	1.67	1.54	2.27
Cost correction factors					
Cost correction for shell type (C$_s$)	0	0	0	0	0
Cost correction for expansion joint (C$_x$)	0	0	0	0	0
Cost correction for tube length (C$_l$)	0	0	0	0.104	0
Cost correction for tube passes (C$_{Ntp}$)	0	0	0	0	0
Cost correction for shell design pressure (C$_{Ps}$)	0	0	0	0.995	1.306
Cost correction for tube design pressure (C$_{Pt}$)	0	0	2.268	2.068	3.157
Cost correction for tube material (C$_{Mtube}$)	1.029	0.604	6.284	8.046	0.591
Cost correction for shell material (C$_{Mshell}$)	0	0	0	0	0
Cost correction for channel material (C$_{Mch}$)	0	0	0	0	0
Cost correction for tubesheet material (C$_{Mts}$)	0	0	0	0	0
Cost correction for tube gauge	−0.138	−0.117	−0.069	−0.089	−0.115
Cost (million euros)					
STHX cost – Original Purohit method	34.43	0.439	2.607	1.678	2.176
STHX cost – Modified Purohit method	19.73	0.293	2.284	1.173	1.434

pressure drop on the tube-side due to the increased diameter, resulting in a net increase in the annualized cost.

Although as previously explained, the theoretically optimal design of a STHX should favour small tube diameters and low or intermediate velocities, as observed in Figs. 6–10, this ideal situation is constrained by construction and manufacturing requirements. These constraints can significantly limit the feasible designs, restricting them to the shaded area shown in these figures. In addition, the final diameter selected is the closest commercial diameter to the one indicated as optimal by the contour graph.

The optimal STHX designs are presented in Table 8, along with the remaining thermal fluid-dynamic parameters for both the shell-side and the tube-side. The final selection of diameters and velocities is conditioned by construction constraints. Only in the case of the HP heat exchangers DIV-CAS and FWH$_2$, where these conditions are less restrictive, does the selected design match the one that minimizes the annualized cost.

As shown in Table 9, the dominant cost factor is the heat transfer area. Consequently, the condenser, being the heat exchanger with the largest area, is also the most expensive. For the same heat exchange area, both the tube-side and shell-side design pressures play a significant role, with higher design pressures resulting in increased costs. Additionally, the material cost has an important impact: DIV-PFC and DIV-CAS heat exchangers are more expensive due to the use of more expensive tube material.

5. Conclusions and recommendations

In this work, a thermo-economic optimization of STHXs has been carried out, applying this methodology to the design calculation of the STHXs in the feedwater line of the DEMO HCPB BoP Power Conversion System.

Compared to other existing works, the proposed methodology presents a detailed analysis of both the thermal fluid-dynamic model (described in Section 2.3) and the cost calculation model (described in Section 2.4). Regarding the thermal fluid-dynamic model, an iterative process has been implemented, based on accurate equations and correlations for both heat transfer and pressure drop calculation. Regarding the economic model, it is important to highlight that the selected methodology leads to more accurate values for STHXs, considering

several design parameters characteristic of this type of heat exchangers.

Furthermore, it is important to note that any heat exchanger optimization model must introduce construction and manufacturing constraints, thus limiting the optimal designs to those that are technically feasible. In this case, the necessary constraints have been introduced, which affect the tube diameter and length, and the shell-to-tube length aspect ratio.

As future work, a thermo-mechanical analysis of the optimal configurations will be carried out. The model will also be extended to other heat exchanger designs, such as compact heat exchangers. In this case, both the thermal fluid-dynamic and economic models would have to be adapted to this type of heat exchanger.

CRediT authorship contribution statement

M.J. Montes: Writing – original draft, Software, Resources, Project administration, Methodology, Investigation, Funding acquisition, Formal analysis, Data curation, Conceptualization. **D. D'Souza:** Writing – review & editing, Validation, Supervision, Software, Investigation. **E. Bubelis:** Writing – review & editing, Visualization, Validation, Supervision, Resources, Data curation, Conceptualization. **S. Perez-Martin:** Writing – review & editing, Visualization, Validation, Supervision, Data curation, Conceptualization.

Declaration of competing interest

The authors declare that they have no known competing financial interests or personal relationships that could have appeared to influence the work reported in this paper.

Acknowledgments

Data availability

Data will be made available on request.

References

[1] R. Aymar, P. Barabaschi, Y. Shimomura, The ITER design, Plasma Phys. Control Fusion. 44 (2002) 519–565, https://doi.org/10.1088/0741-3335/44/5/304.

[2] A. Woods, A. Hellend, J. Keep, E. Kimbrey, J. Hagues, Approach to spatial integration on a novel and complex major project – STEP concept Tokamak, Fusion Eng. Des. 202 (2024) 114347, https://doi.org/10.1016/j.fusengdes.2024.114347.

[3] B.N. Sorbom, J. Ball, T.R. Palmer, F.J. Mangiarotti, J.M. Sierchio, P. Bonoli, C. Kasten, D.A. Sutherland, H.S. Barnard, C.B. Haakonsen, J. Goh, C. Sung, D. G. Whyte, ARC: a compact, high-field, fusion nuclear science facility and demonstration power plant with demountable magnets, Fusion Eng. Des. 100 (2015) 378–405, https://doi.org/10.1016/j.fusengdes.2015.07.008.

[4] G. Federici, J. Holden, C. Baylard, A. Beaumont, The EU DEMO staged design approach in the pre-concept design phase, Fusion Eng. Des. 173 (2021) 112959, https://doi.org/10.1016/j.fusengdes.2021.112959.

[5] L. Barucca, E. Bubelis, S. Ciattaglia, A. D'Alessandro, A. Del Nevo, F. Giannetti, W. Hering, P. Lorusso, E. Martelli, I. Moscato, A. Quartararo, A. Tarallo, E. Vallone, Pre-conceptual design of EU DEMO balance of plant systems: objectives and challenges, Fusion Eng. Des. 169 (2021) 112504, https://doi.org/10.1016/j.fusengdes.2021.112504.

[6] S. Ciattaglia, G. Federici, L. Barucca, R. Stieglitz, N. Taylor, EU DEMO safety and balance of plant design and operating requirements. Issues and possible solutions, Fusion Eng. Des. 146 (2019) 2184–2188, https://doi.org/10.1016/j.fusengdes.2019.03.149.

[7] L. Barucca, W. Hering, S. Perez Martin, E. Bubelis, A. Del Nevo, M. Di Prinzio, M. Caramello, A. D'Alessandro, A. Tarallo, E. Vallone, I. Moscato, A. Quartararo, S. D'amico, F. Giannetti, P. Lorusso, V. Narcisi, C. Ciurluini, M.J. Montes Pita, C. Sánchez, A. Rovira, D. Santana, P. Gonzales, R. Barbero, M. Zaupa, M. Szogradi, S. Normann, M. Vaananen, J. Ylatalo, M. Lewandowska, L. Malinowski, E. Martelli, A. Froio, P. Arena, A. Tincani, Maturation of critical technologies for the DEMO balance of plant systems, Fusion Eng. Des. 179 (2022) 113096, https://doi.org/10.1016/j.fusengdes.2022.113096.

[8] L. Barucca, S. Ciattaglia, M. Chantant, A. Del Nevo, W. Hering, E. Martelli, I. Moscato, Status of EU DEMO heat transport and power conversion systems, Fusion Eng. Des. 136 (2018) 1557–1566, https://doi.org/10.1016/j.fusengdes.2018.05.057.

[9] E. Gaio, A. Ferro, A. Maistrello, M. Dan, F. Lunardon, L. Barucca, S. Ciattaglia, G. Federici, I. Benfatto, The EU DEMO plant electrical system: issues and perspective, Fusion Eng. Des. 156 (2020) 111728, https://doi.org/10.1016/j.fusengdes.2020.111728.

[10] F. Cismondi, G.A. Spagnuolo, L.V. Boccaccini, P. Chiovaro, S. Ciattaglia, I. Cristescu, C. Day, A. Del Nevo, P.A. Di Maio, G. Federici, F. Hernandez, C. Moreno, I. Moscato, P. Pereslavtsev, D. Rapisarda, A. Santucci, M. Utili, Progress of the conceptual design of the European DEMO breeding blanket, tritium extraction and coolant purification systems, Fusion Eng. Des. 157 (2020) 111640, https://doi.org/10.1016/j.fusengdes.2020.111640.

[11] G. Mazzone, J.-H. You, C. Bachmann, U. Bonavolontà, V. Cerri, D. Coccorese, D. Dongiovanni, D. Flammini, P. Frosi, L. Forest, G. Di Gironimo, G. Di Mambro, V. Imbriani, A. Maffucci, D. Marzullo, P.A. Di Maio, M.T. Porfiri, E. Vallone, R. Villari, E. Visca, C. Vorpahl, Eurofusion-DEMO Divertor - cassette design and integration, Fusion Eng. Des. 157 (2020) 111656, https://doi.org/10.1016/j.fusengdes.2020.111656.

[12] R. Mozzillo, C. Bachmann, G. Aiello, D. Marzullo, Design of the European DEMO vacuum vessel inboard wall, Fusion Eng. Des. 160 (2020) 111967, https://doi.org/10.1016/j.fusengdes.2020.111967.

[13] S. Perez-Martin, E. Bubelis, W. Hering, L. Barucca, R&D needs for the design of the EU-DEMO HCPB ICD balance of plant in FP9, J. Nucl. Eng. 3 (2022) 435–445.

[14] I. Moscato, L. Barucca, E. Bubelis, G. Caruso, S. Ciattaglia, C. Ciurluini, A. Del Nevo, P.A. Di Maio, F. Giannetti, W. Hering, P. Lorusso, E. Martelli, V. Narcisi, S. Norrman, T. Pinna, S. Perez-Martin, A. Quartararo, M. Szogradi, A. Tarallo, E. Vallone, Tokamak cooling systems and power conversion system options, Fusion Eng. Des. 178 (2022) 113093, https://doi.org/10.1016/j.fusengdes.2022.113093.

[15] Manohar S. Sohal, Matthias A. Ebner, Piyush Sabharwall, Phil Sharpe, 2010. Engineering database of liquid salt thermophysical and thermochemical properties (No. INL/EXT-10-18297, 980801). https://doi.org/10.2172/980801.

[16] C.S. Turchi, J. Vidal, M. Bauer, Molten salt power towers operating at 600–650 °C: salt selection and cost benefits, Sol. Energy 164 (2018) 38–46, https://doi.org/10.1016/j.solener.2018.01.063.

[17] E. Bubelis, S. Ruck, Design update of DEMO BoP for HCPB BB concept with an energy storage system, Fusion Eng. Des. 206 (2024) 114610, https://doi.org/10.1016/j.fusengdes.2024.114610.

[18] I. Moscato, CCB1-1 DEMO thermal power flow configurations: reference & study variants. Inputs for tokamak coolant systems and BoP systems, So-Call. Energy Map (2021). IDM reference: EFDA_D_2P6G7T, v1.0.

[19] G.P. Purohit, Estimating the cost of shell-and tube heat exchangers, Chem. Eng. 90 (1983) 56–67.

[20] S. Kakaç, H. Liu, A. Pramuanjaroenkij, Heat Exchangers: Selection, Rating, and Thermal Design. Ed, 3rd Edition, Taylor & Francis, 2012. ISBN: 978-1- 4398-4990-3.

[21] S.Boilers Kakaç, Evaporators, and Condensers. Ed, ISBN, John Wiley & Sons, 1991, pp. 978–0471621706.

[22] Standards of the Tubular Exchanger Manufacturers Association, TEMA (Tubular Exchanger Manufacturers Association), 8th edition, Tarrytown, NY, 1999.

[23] A.C. Caputo, P.M. Pelagagge, P. Salini, Heat exchanger design based on economic optimisation, Appl. Therm. Eng. 28 (2008) 1151–1159, https://doi.org/10.1016/j.applthermaleng.2007.08.010.

[24] M. Asadi, Y. Song, B. Sunden, G. Xie, Economic optimization design of shell-and-tube heat exchangers by a cuckoo-search-algorithm, Appl. Therm. Eng. 73 (2014) 1032–1040, https://doi.org/10.1016/j.applthermaleng.2014.08.061.

[25] Energy Information Administration (EIA), 2024. Electric Power annual 2024. Average retail price of electricity to ultimate consumers by end-use sector. www.eia.doe.gov.

[26] https://world-nuclear.org/information-library/economic-aspects/economics-of-nuclear-power.

[27] R.S. Hall, J. Matley, K.J. McNaughton, Current costs of process equipment, Chem. Eng. (1982) 80–116.

[28] P.A. González-Gómez, F. Petrakopoulou, J.V. Briongos, D. Santana, Cost-based design optimization of the heat exchangers in a parabolic trough power plant, Energy 123 (2017) 314–325, https://doi.org/10.1016/j.energy.2017.02.002.

[29] D.R. Woods, Rules of Thumb in Engineering Practice, 1st ed., Wiley, 2007 https://doi.org/10.1002/9783527611119.

[30] M. Taal, Cost estimation and energy price forecasts for economic evaluation of retrofit projects, Appl. Therm. Eng. 23 (2003) 1819–1835, https://doi.org/10.1016/S1359-4311(03)00136-4.

[31] Schmitt, T., Leptinsky, S., Turner, M., Zoelle, A., White, C., Hughes, S., Homsy, S., Woods, M., Hoffman, H., Shultz, T., James Iii, R., 2022. Cost and performance baseline for fossil energy plants volume 1: bituminous coal and natural gas to electricity (No. DOE/NETL-2023/4320, 1893822). https://doi.org/10.2172/1893822.

[32] Chemical engineering plant cost index, http://www.chemengonline.com/pci-home.